Waste Technology (WasTech)
Journal homepage: http://ejournal.undip.ac.id/index.php/wastech
An International Journal

Sustainable Batik Wastewater Treatment using Advanced PVDF/NiFe@SiO_2 Nanocomposite Photocatalytic Membrane

Tutuk Djoko Kusworo, Budiyono, Siswo Sumardiono

Department of Chemical Engineering, Faculty of Engineering, Universitas Diponegoro, Indonesia
Email: tdkusworo@che.undip.ac.id

Abstract - *The primary concern associated with the Batik industry lies in the presence of pollutant dyes that contribute to environmental contamination. Addressing this issue involves exploring various wastewater treatment methods, with membrane technology being a viable approach. In this study, a photocatalytic material, NiFe@SiO_2, synthesized through the sol-gel technique, was incorporated into a PVDF membrane. Characterization results from SEM surface, indicated that the PVDF/NiFe@SiO_2 membrane displayed superior characteristics compared to other membranes. The addition of the NiFe@SiO_2 photocatalyst increased membrane porosity, hydrophilicity, water absorption capacity, and affinity towards water molecules. The PVDF/NiFe@SiO_2 membrane exhibited enhanced performance in terms of permeate flux, pollutant rejection, stability, recyclability, and durability. Notably, the fabricated photocatalytic membrane demonstrated superior antifouling performance and flux recovery capability when operating under UV radiation. The study also delved into the influence of wastewater pretreatment on antifouling membrane performance. The modified membrane successfully reduced fouling levels on the membrane by enhancing FRR from ~70% to ~90%. This insight into how pretreatment affects the antifouling properties of wastewater opens avenues for innovative solutions and enhanced design strategies to improve the efficiency and sustainability of wastewater treatment processes. Future research endeavors could focus on maximizing the potential of the bentonite adsorbent in wastewater pretreatment and exploring the full capabilities of the NiFe@SiO_2 photocatalyst in enhancing the photocatalytic and antifouling performance of the membrane.*

Keywords *– Batik wastewater, Fouling, Membrane, Nickel ferrite, Photocatalytic*
Doi: http://dx.doi.org/10.14710/wastech.12.1.1-9
[How to cite this article: Kusworo, et al. (2024). Sustainable Batik Wastewater Treatment using Advanced PVDF/NiFe@SiO_2 Nanocomposite Photocatalytic Membrane, 10(1), 7-16 doi: http://dx.doi.org/10.14710/wastech.12.1.1-9]

1. Introduction

Due to the surging popularity of batik, Indonesia's batik industry has undergone substantial expansion [1]. The primary concern associated with the batik industry revolves around the discharge of wastewater generated during soaking, boiling, and rinsing processes [2]. This batik wastewater contains persistent synthetic dyes, particularly challenging to degrade, including heavy metals such as Cd, Cr, Pb, Co, Cu, Hg, Ni, Mg, Fe, and Mn. These metals enhance the bond strength between dyes and fabric [3], [4]. The pollutants in batik wastewater, including residual dyes, catalytic chemicals (wax, sodium silicate as a binding agent), excess nutrients (nitrogen, phosphorus), and organic matter (sodium, potassium, magnesium, calcium, copper, lead, nickel, and zinc), result in elevated levels of pH, chemical oxygen demand (COD), biological oxygen demand (BOD), total dissolved solids (TDS), total suspended solids (TSS), and high color intensity [5], [6]. Contaminated water from batik wastewater poses a threat to human health [7].

Given the environmental and health impacts of batik waste, it is imperative to explore effective methods to mitigate these adverse effects on human life [8]. Although biological processes are frequently employed, their limited ability to degrade dye compounds from wastewater renders them inefficient. Membrane technology emerges as an effective approach for wastewater treatment due to its straightforward operation, high productivity, absence of additional chemical additives, and classification as a clean technology [9]. However, this technology faces challenges, notably compromised membrane separation efficiency due to issues like concentration polarization and membrane fouling. Membrane fouling, the irreversible deposition of suspended or dissolved solids on the external surface or pores of the membrane, impedes overall membrane performance. Once fouled, complex and often expensive cleaning steps are required, impacting the continuous

operation of the membrane filtration process, including forward and reverse flushing, backwashing, air scouring, and back permeation [10].

Fouling caused by colorants as foulants can be alleviated on membranes through photocatalytic reactions [11]. However, practical photocatalytic applications demand adequate light intensity surpassing the energy bandgap of the photocatalyst. Silicone dioxide (SiO_2) has gained significant attention in photocatalysis due to its facile synthesis, unique structure, and various functional groups. SiO_2's photocatalytic activity stems from its semiconductor behavior with an absorption band around 280 nm [12]. Transition metals or noble metals like iron (Fe) and nickel (Ni) facilitate electron trapping, suppressing electron-hole recombination, and enhancing photocatalytic activity. Nickel (Ni) exhibits good activity and is more cost-effective than noble metals, making it widely used in various applications due to its physicochemical properties. Iron (Fe), with its half-filled electron configuration ($3d^5$) and similar ionic radius to Ti^{4+}, functions as shallow charge traps [13].

Therefore, in this investigation, a PVDF membrane was incorporated with NiFe@SiO_2 composite using the sol-gel method to enhance the photocatalytic and antifouling performance of the membrane, achieving a more homogeneous distribution of the photocatalytic material. This resulted in improved membrane filtration processes for the treatment of batik wastewater to produce clean water. The membrane's characteristics were initially assessed through SEM, XRD, FTIR, contact angle, and porosity analyses. The impact of adding the NiFe@SiO2 composite on photocatalytic and antifouling performance was evaluated under ultraviolet light.

2. Materials and Methods

2.1 Materials

Materials and chemicals used in this research were real Batik wastewater from local industries in Semarang, PVDF (*polyvinylidene fluoride*) (Sigma-Aldrich Corporation, Germany), N-methyl-2-pirrolidone (Merck), Pure iron powder (Merck), Pure nickel powder 95-97% (Merck), SiO_2 NP *(silica nanoparticles)* (Merck), demineralized water (produced in laboratory), HCl (*hydrochloric acid*) (Merck), and Bentonit (Indrasari Chemicals).

2.2 Synthesis of NiFe@SiO_2

Nanocomposite NiFe@SiO_2 was prepared via sol-gel method by adapting and modifying the method from prior studies [14]. Initially, 50 grams of SiO2 were introduced into 250 mL of 2M NaOH solution and stirred using a magnetic stirrer at 150°C for a duration of 2 hours. The solution was subsequently cooled to room temperature, and the insoluble SiO2 was filtered and separated. Following this, 100 mL of the solution was combined with 5 grams of Ni, Fe, and NiFe powders. A 1M HCl solution was incrementally added dropwise via a buret while stirring with a magnetic stirrer until a white gel formed. Once gel formation occurred, the solution underwent filtration and was left to stand for 24 hours to allow for gel compaction. The compacted gel was subjected to drying in an oven at 110°C and then crushed using a Ball Milling-Sieving Mesh apparatus to obtain powder.

2.3 Fabrication of nanocomposite membranes

The formulation of the casting solution involved a combination of 16 wt.% PVDF and 84 wt.% of N-methyl-2-pyrrolidone (NMP) as the control variable. To examine the impact of introducing photocatalysts NiFe@SiO_2 on membrane performance, different concentrations of this photocatalyst was investigated by varying their amounts in the casting solution, maintaining a mass basis of 50 grams. The dispersion of the photocatalysts was achieved by using an ultrasonic apparatus for 1 hour, incorporating a portion of NMP as the dispersing agent. Subsequently, the dispersed solution underwent mixing with PVDF and the remaining NMP using a magnetic stirrer at 70°C for a duration of 10 hours to achieve a uniform solution. This homogeneous casting solution was allowed to stand for 12 hours at room temperature to eliminate any residual bubbles. The membrane was cast employing the dry-wet phase inversion method by pouring the casting solution onto a casting knife positioned on a glass plate. The casting knife was then moved parallel to the glass plate, forming a thin layer on the plate, and was subsequently immersed in a coagulation tank containing water, left to stand at room temperature for 1 day. Finally, the membrane was dried either overnight at 30°C or at room temperature [15]. The design detailing the variation in photocatalyst concentration in the membrane is presented in the following Table 1.

Table 1 Design of variation in photocatalyst concentration in the casting solution

Membrane	PVDF (wt.%)	NMP (wt.%)	PVP (wt.%)	NiFe@SiO_2 (wt.% in TS)
PV0	16	84	2	0
PVNFS01	16	84	2	1
PVNFS02	16	84	2	2
PVNFS03	16	84	2	3
PVNFS04	16	84	2	4

2.4 Membrane performance evaluation

Evaluation of membrane performance was performed for treating Batik wastewater. The filtration process is executed using a cross-flow system membrane module, as illustrated in Figure 1. The composite membrane is positioned in the filter area and subsequently compressed using demineralized water for a duration of 30 minutes. Subsequently, wastewater is introduced to the membrane under a pressure of 5 bar. The collected permeate water is measured for volume at intervals of 30 minutes. An analysis of the pollutant content in the permeate water is conducted

to assess the membrane separation performance. The permeate flux is computed using equation (1).

$$J = \frac{V}{A \times t} \quad (1)$$

Where J is permeate flux (L.m^{-2}.h^{-1}), V is permeate volume (L), A is membrane surface area (m^2), and t is filtration time (hours).

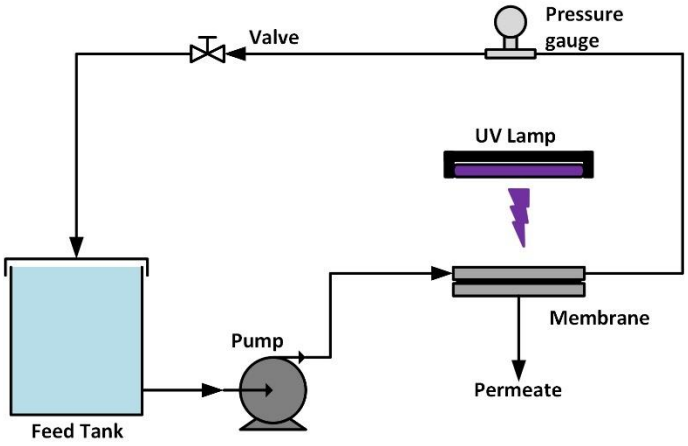

Figure 1. Membrane filtration cell for experiment

Rejection (R) is defined as a measure of the ability of a membrane to retain or pass certain components (Murni and Sudarmi, 2010). In this study, rejection was based on the ability to retain total dissolved solids (TDS), Chemical Oxygen Demand (COD), and color of Batik wastewater. The rejection coefficient is the fraction of solute concentration that does not penetrate the membrane and is expressed in equation (2):

$$R = \left(1 - \frac{C_P}{C_f}\right) \times 100\% \quad (2)$$

Where R is pollutant rejection (%), CP and Cf are concentrations of solutes (contaminants) in the permeate and feed.

2.5 Nanocomposite membrane characterization

Characterization tests are carried out to assess the properties of both the photocatalyst and the membrane. For the photocatalyst, various tests, including Fourier Transform Infrared Spectroscopy (FTIR), X-Ray Diffraction (XRD), and UV-Vis Diffuse Reflectance Spectroscopy (UV-Vis DRS), are employed. To characterize the membrane, a range of tests are conducted, including Scanning Electron Microscope Surface (SEM Surface), Scanning Electron Microscopy-Energy Dispersive X-Ray (SEM-EDX), Contact Angle, Porosity, and Mechanical Strength.

SEM Surface characterization is utilized to observe the morphology and pore size of the membrane. SEM-EDX testing is employed to investigate the topography (surface and texture), morphology (shape and size), and composition of the analyzed sample [16]. In addition to SEM, FTIR characterization is carried out to identify changes in organic functional groups [17]. XRD testing is performed to discern the structure and crystal identification [18], while contact angle testing determines the hydrophobicity and hydrophilicity properties of the membrane [15]. Porosity testing reveals the number of substances or components that can be absorbed by the membrane [19], and mechanical strength testing provides information on the mechanical properties of the membrane, including tensile strength and elongation. UV-Vis DRS characterization is linked to the photocatalytic properties of the catalyst added to the membrane, supplying information about the bandgap width [20].

2.6 Membrane Fouling Analysis

The evaluation of antifouling potential is examined to obtain the total fouling ratio (Rt, %), reversible fouling ratio (Rr, %), irreversible fouling ratio (Rir, %), and flux recovery ratio (FRR, %) using the following formulas:

$$R_t = \frac{J_{pw0} - J_{ww}}{J_{pw0}} \times 100\% \quad (3)$$

$$R_r = \frac{J_{pw1} - J_{ww}}{J_{pw0}} \times 100\% \quad (4)$$

$$R_{ir} = \frac{J_{pw0} - J_{pw1}}{J_{pw0}} \times 100\% \quad (5)$$

$$F_{RR} = \left(\frac{J_{pw1}}{J_{pw0}}\right) \times 100\% \quad (6)$$

3. Results and Discussion

3.1 Morphological properties using SEM analysis

SEM images of the surface and cross-sectional morphology of the pristine PVDF and PVDF/NiFe@SiO_2 nanocomposite membrane are shown in Figure 2. The images depict the surface topography of the membranes at magnifications of 1000x. The PVDF neat membrane showcases a smooth and uniform surface without pores or agglomerations, suggesting the homogeneous mixing of the PVDF polymer with the solvent and resulting in a compact membrane structure [21]. In membranes with the addition of NiFe@SiO_2, the membrane surfaces exhibit asymmetry with fiber entanglements and larger pore sizes compared to the PVDF neat membrane. The introduction of photocatalysts also contributes to agglomeration within the membrane structure, indicating a random distribution of material particles within the membrane. A high concentration of agglomeration can diminish the strength and modulus of the membrane, acting as a stress concentrator and reducing interfacial concentration [22]. The NiFe@SiO_2 nanoparticles are available on the membrane surface that can lead the improvement of photocatalytic activity due to direct UV light access. The PVDF neat membrane exhibits a smooth and flat surface, while the PVDF/NiFe@SiO_2 membrane appears rougher. The addition of photocatalysts influences the formation of a rougher surface on the membrane. This can be attributed to changes in the interaction between solvents and non-solvents, as well as the agglomeration of photocatalysts

during the phase inversion process and the presence of relative porosity. Furthermore, pore blockage by photocatalysts may reduce the effectiveness of pore structure formation and affect the surface roughness [23]. The formation of a rougher surface in the PVDF/NiFe@SiO_2 membrane compared to the PVDF neat membrane indicates the presence of NiFe@SiO_2 photocatalysts within the membrane. These alterations in surface morphology affirm the successful integration of photocatalysts into the membrane.

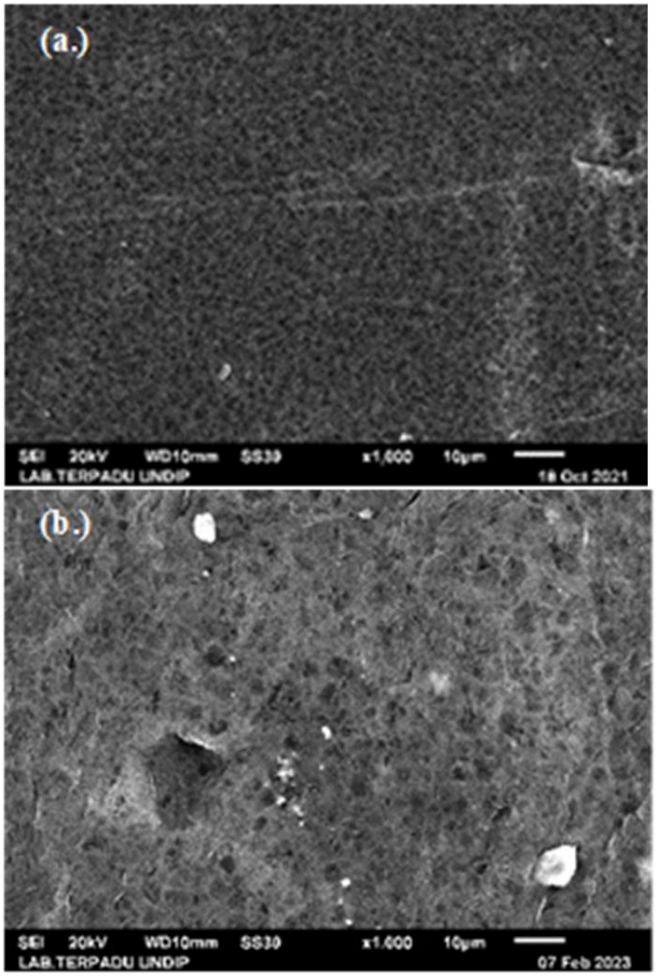

Figure 2. SEM images of (a) pristine PVDF membrane (b) PVDF/NiFe@SiO_2 nanocomposite membrane

3.2 FTIR and XRD pattern analysis

In Figure 3, the FTIR spectra of the neat PVDF membrane exhibits peaks at wavenumbers of 900-800 cm^{-1}, which correspond to the C-C bond stretching vibrations [24]. The peak at 1401 cm^{-1} indicates the -CH_2 stretching vibration, while the peaks at 1180 cm^{-1} and 1280 cm^{-1} represent the C-F and C-F_2 stretching vibrations, respectively [25]. Meanwhile, The NiFe@SiO_2 photocatalyst shows a broad peak at 3455 cm^{-1}, corresponding to the O-H stretching vibration. A prominent peak is observed at 594 cm^{-1}, which is a characteristic peak of metal oxide materials, specifically Ni-O and Fe-O bonds [24]. The FTIR spectra of PVDF/NiFe@SiO_2 appears as a combined spectrum of PVDF neat and NiFe@SiO_2. In Figure 3, a small peak is observed around 3020 cm^{-1}, indicating the O-H molecular vibration due to the addition of hydrophilic nanofillers. Meanwhile, based on Figure 3, the peak at 1403 cm^{-1} corresponds to the C=C bond of PVDF backbone, and the peak at 601 cm^{-1} corresponds to the vibrations of oxide groups in the NiFe@SiO_2 photocatalyst, such as Ni-O and Fe-O. These findings further indicate the successful integration of the NiFe@SiO_2 photocatalyst into the PVDF/NiFe@SiO_2 membrane matrix.

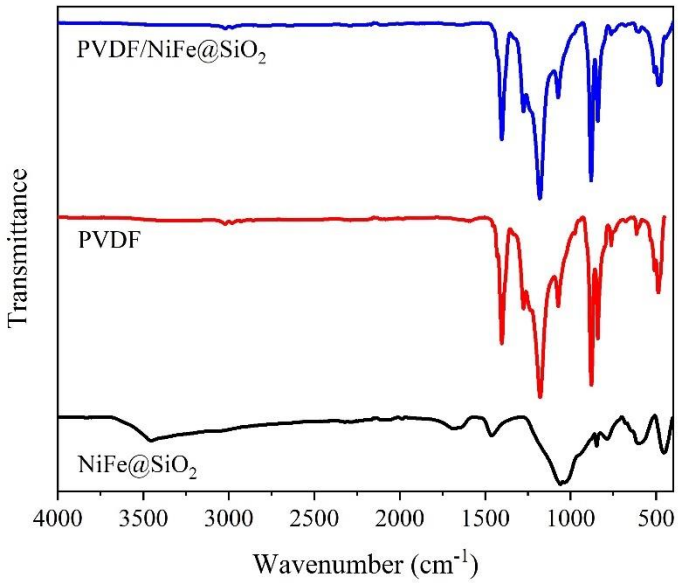

Figure 3. FTIR spectra of fabricated membranes and photocatalyst

To strengthen the evidence of successful incorporation of NiFe@SiO_2 in the membrane, XRD analysis was performed. The diffractograms in Figure 4 depict the XRD analysis results at diffraction angles ranging from 10 to 70°. The XRD pattern of PVDF neat (Figure 8c) predominantly displays an amorphous structure. The broad peaks observed at diffraction angles between 15 and 250 exhibit the characteristic features of PVDF polymer [24]. There are two prominent peaks at 18.76° and 20.18° indicating the α-phase of PVDF polymer. The α-phase PVDF is the common structure of PVDF with the lowest dipole moment, therefore it is categorized as nonpiezoelectric polymer. In contrast, in the PVDF/NiFe@SiO_2 membrane, a broad peak around 20 - 40° with strong peak at 30.88° is correspond to the characteristic diffraction pattern of β-phase PVDF. β-phase PVDF has the most significant piezoelectric properties among the polymorphs due to its polar chains. Furthermore, several new peaks are identified, namely small peaks at 35.82°, 43.71°, and 50.36° corresponding to the presence of NiFe@SiO_2 photocatalyst. The observed XRD pattern matches the literature reports, indicating that the crystal structure of NiFe@SiO_2 is predominantly composed of spinel ferrite Ni [24]. The introduction of NiFe@SiO_2 into PVDF matrix could be the

possible reason in altering the α-PVDF into β-PVDF. The positive charge of Ni and Fe interact with fluoride group in PVDF molecule to form separated charge in PVDF molecule. This phenomenon is beneficial in membrane operation as the molecular charge of PVDF can contribute in charge exclusion of electrostatic charged pollutant particles. Furthermore, several studies revealed that electrostatic repulsion has strong influence in mitigating fouling tendency [26].

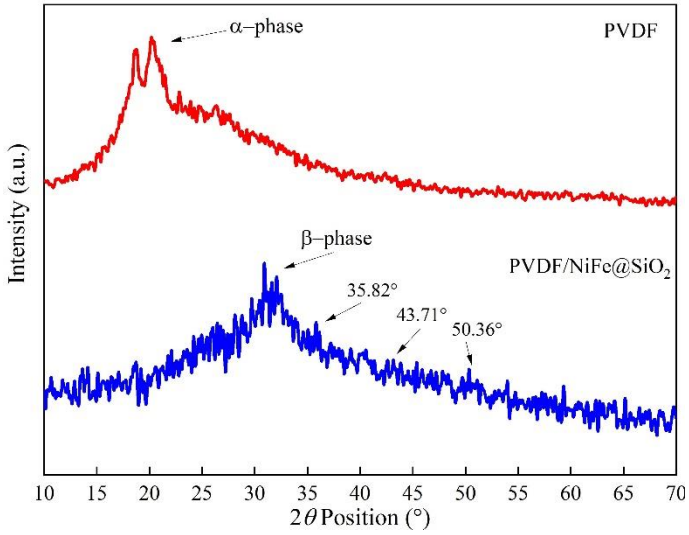

Figure 3. XRD pattern of fabricated membranes

3.3 Membrane water contact angle and pore properties

The contact angle between the membrane surface and a liquid can indicate the hydrophilic or hydrophobic nature of the membrane. A hydrophilic membrane has a contact angle of less than 90°, while a contact angle greater than 90° indicates a hydrophobic membrane [27]. Hydrophilicity can enhance the membrane's ability to allow water molecules to pass through the pores, thereby influencing the flux value and permeability rate in filtration processes [28], [29], and it can also prevent fouling on the membrane surface [30]. Based on the analysis in Table 2, the PVDF neat membrane exhibits low hydrophilicity with a contact angle greater than 90°, specifically 108.27°. The addition of NiFe@SiO_2 at 1.0 and 2.0 wt.% to the membrane visibly enhances its hydrophilicity compared to PVDF neat. This is evident from the decrease in the contact angle on the membrane surface to 94.18° and 86.56°, respectively, due to the formation of hydrophilic (-OH) groups within the membrane structure, thereby increasing its ability to interact with water [29], [31]. Meanwhile, membranes with the addition of NiFe@SiO_2 at higher concentration of 3.0 wt.% and 4.0 wt.% show an increase in the contact angle compared to neat PVDF, i.e., 95.21°, and 89.44°, respectively. This is attributed to the formation of agglomerate of nanoparticles due to the overloading of NiFe@SiO_2, which can increase the membrane roughness thereby increasing the water contact angle [32].

Tabel 2. Water contact angle, porosity, and mean pore radius

Membrane	Contact angle (°)	Porosity (%)	Pore radius (nm)
PV0	108.27 ± 1.35	51.3	7.64
PVNFS01	94.18 ± 2.23	62.7	8.00
PVNFS02	86.56 ± 1.47	67.5	9.00
PVNFS03	95.21 ± 3.14	69.3	11.63
PVNFS04	89.44 ± 2.28	74.4	9.37

Membrane porosity is a structural property responsible for maintaining membrane permeability. The higher the porosity of a membrane, the greater its permeability. The analysis results show that the membrane porosity gradually increases with the sequential addition of photocatalysts loading concentration: 51.3%, 62.7%, 67.5%, 69.3%, and 74.4% for PVDF neat, PVDF with NiFe@SiO_2 incorporation at 1.0; 2.0; 3.0; and 4.0 wt.%, respectively. The value of porosity indicates the level of available void space within the membrane. Membranes with lower porosity indicate denser structures, while membranes with higher porosity have a higher void space within the membrane. The addition of photocatalysts creates void spaces during the phase inversion process, resulting in gaps between the polymer matrix and photocatalysts [24].

Additionally, the average pore radius of the membrane was evaluated using the Guerout-Elford-Ferry approach. Based on Table 5, the PVDF neat membrane exhibited the smallest average pore radius, and the addition of photocatalysts increased the average pore radius of the membrane. This increase is attributed to the appearance of gaps within the polymer matrix due to the addition of photocatalysts. The measured values were 7.64, 8.00, 9.00, 11.63, 9.37, and 7.71 nm for PVDF neat, PVDF with NiFe@SiO_2 incorporation at 1.0; 2.0; 3.0; and 4.0 wt.%, respectively. The pore sizes of all membranes are within the range of 5-100 nm, classifying them as ultrafiltration (UF) membranes [32].

3.4 Membrane Performance Evaluation

According to the evaluation of flux performance depicted in Figure 4, the PVDF membrane incorporating 4.0 wt.% of NiFe@SiO_2 demonstrates the highest flux value compared to other membranes. It starts with an initial flux value of 29.90 $L.m^{-2}.h^{-1}$, gradually decreasing to 20.68 $L.m^{-2}.h^{-1}$ over time. The introduction of NiFe@SiO_2 photocatalyst in the PVDF membrane significantly influences water permeation, retention potential, and fouling resistance. The concentration of NiFe@SiO_2 in the membrane positively correlates with flux, as evidenced by the higher flux in the PVDF membrane with 4.0 wt.% NiFe@SiO_2 compared to the PVDF membrane with 1.0 wt.% NiFe@SiO_2. The modification of membrane structure through photocatalyst addition increases membrane porosity, leading to improved water permeability and flux.

This phenomenon corresponds with previous result where 4 wt.% photocatalyst loading creates membrane with the highest porosity and relatively larger pore size radius. The reduction in the upper layer also contributes to enhanced permeation properties. Additionally, the improvement in permeate flux was further attributed to the photocatalysis process. In photo-irradiated membrane filtration, the photocatalyst induces the generation of reactive oxygen species (ROS), which actively degrade pollutants. Simultaneously, the presence of ROS results in the formation of a hydration layer that attracts water molecules, thereby augmenting permeate flux. This dual mechanism, involving both pollutant degradation and the creation of a water-attracting layer, contributes to the overall enhancement of permeate flux during the photo-irradiated membrane filtration process.

According to Table 3, the PVDF/NiFe@SiO_2 at 2 wt.% loading concentration achieves the highest rejection for both TDS and dyes, with rejection values of 55.18% and 90.28%, respectively. For COD rejection, the PVDF/NiFe@SiO_2 1.0 wt.% membrane exhibits the highest rejection at 71.12%, surpassing PVDF/NiFe@SiO_2 2.0 wt.% and neat PVDF with rejection values of 63.18% and 30.13 %, respectively. Despite this, average rejection values indicate that the PVDF/NiFe@SiO_2 2.0 wt.% membrane outperforms the PVDF/NiFe@SiO_2 1.0 wt.% membrane and neat PVDF. This superior performance is attributed to the membrane's surface hydrophilicity, with hydrophilic sites from hydroxyl, carbonyl, and carboxyl functional groups attracting water more effectively due to their similar polarity. The rejection performance improvement is a result of this enhanced hydrophilicity. However, it's noted that excessive photocatalyst addition may lead to agglomeration and potential damage to membrane pores, compromising rejection performance. Other possible reasons are the influence of photocatalytic activity of membrane under UV irradiation. The generated ROS helps degrading organic pollutant and dyes. However, the higher photocatalyst loading into membrane significantly decrease the rejection of COD and dyes. It could be due to the formation of agglomerates that limits the irradiation access. The PVDF/NiFe@SiO_2 2.0 wt.% membrane emerges as the optimal concentration for NiFe@SiO_2 addition, exhibiting the highest values in both flux and rejection performance.

Table 3. Rejection efficiencies of fabricated membrane in Batik wastewater treatment

Membrane	Rejection (%)		
	TDS	COD	Dyes
PV0	38.27	30.13	61.22
PVNFS01	52.31	71.12	79.38
PVNFS02	55.18	63.18	90.28
PVNFS03	54.14	60.33	82.18
PVNFS04	54.77	56.72	84.38

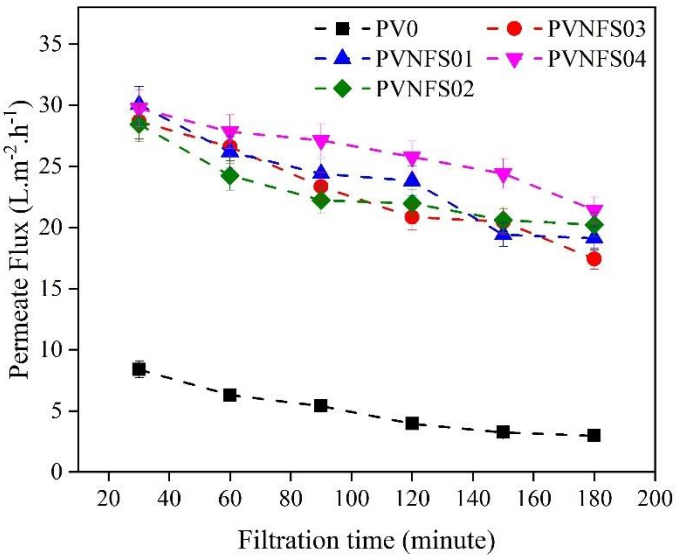

Figure 4. Permeate fluxes of fabricated membranes under UV irradiation

3.4 Membrane Fouling Evaluation

Fouling poses a significant challenge in membrane technology, where the accumulation of foulants on the membrane surface leads to a decline in performance. To comprehensively assess the antifouling properties of membranes, various parameters such as total fouling (Rt), reversible fouling (Rr), irreversible fouling (Rir), and flux recovery ratio (FRR) are introduced and evaluated. Figure 5 presents the values of Rt, Rr, Rir, and FRR for all membranes, with and without UV radiation, following fouling with batik wastewater. Higher FRR values generally indicate better antifouling characteristics, and all hybrid membranes exhibit higher FRR values compared to the neat PVDF membrane, indicating improved antifouling properties. The neat PVDF membrane with UV radiation shows a low FRR of 53.95%, signifying poor antifouling properties. The incorporation of photocatalysts, including NiFe@SiO_2 at 1.0; 2.0; 3.0; and 4.0 wt.% tends to increase FRR, with the highest FRR value (79.4%) observed in the PVDF/NiFe@SiO_2 membrane with 3.0 wt.% loading. In dark conditions, hydrophilicity and surface properties such as roughness play a crucial role in membrane performance and fouling mitigation, where hydrophilic surfaces demonstrate better antifouling abilities. When compared to hybrid membranes without UV radiation, those with UV radiation exhibit enhanced FRR due to potential photocatalytic degradation. The fouling ratio decreases significantly while FRR increases, indicating effective reduction of fouling formation. In the best-case scenario with the PVDF/NiFe@SiO_2 membrane, FRR increases from 79.4% to 90.02%, suggesting an improvement in antifouling properties through the combination of NiFe@SiO_2 under UV radiation.

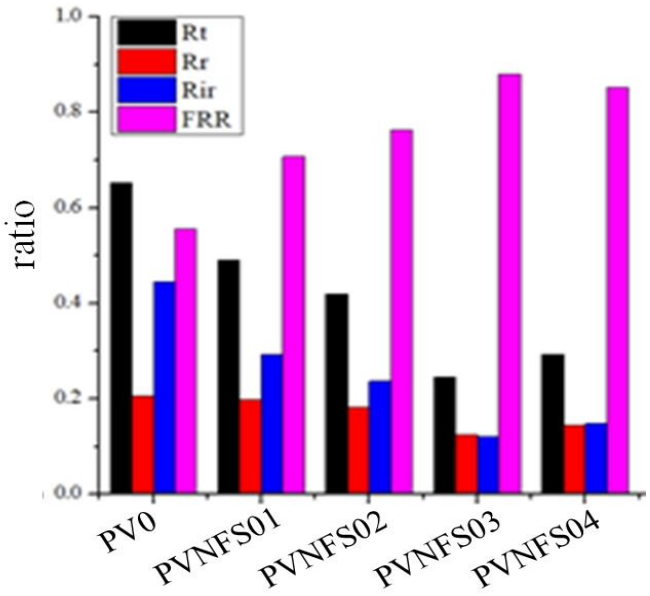

Figure 5. Flux recovery ratio and fouling ratios

Fouling can be divided into reversible fouling caused by loose protein adsorption on the membrane surface and irreversible fouling caused by protein deposition on the surface or trapping within membrane pores. A recent study found that UV-treated photocatalytic membranes exhibit a higher ratio of reversible fouling to total fouling (Rr/Rt) and a lower ratio of irreversible fouling to total fouling (Rir/Rt), indicating effective resistance to irreversible foulants due to the photocatalytic activity on the membrane surface, known to be more challenging to remove than reversible foulants. Overall, the results highlight that the PVDF/NiFe@SiO_2 membrane demonstrates superior photocatalytic antifouling behavior compared to other membranes, positioning it as a promising candidate for applications in the antifouling field.

5. Conclusion

The concentrations of added photocatalysts that yield the best combination to gain highest flux performance and rejection are determined to be 2 wt.% of NiFe@SiO_2. This concentration result in membranes with enhanced surface area, porosity, and hydrophilicity. Additionally, the membranes exhibit the formation of Ni-O, Fe-O, and Si-O, oxide compositions. The modified PVDF/NiFe@SiO_2 membrane demonstrates the β-phase PVDF that beneficial in charge exclusion mechanism. The notable photocatalytic performance was observed showcasing higher flux performance and rejection during UV-irradiated filtration. The increased FRR in the modified PVDF/NiFe@SiO_2 membrane further indicates an improved antifouling membrane performance. This suggests that the selected concentrations of photocatalysts contribute to the creation of membranes with favorable characteristics, leading to enhanced filtration efficiency, resistance to fouling, and improved overall performance in UV-irradiated conditions.

References

[1] Sharfan, N., Shobri, A., Anindria, F.A., Mauricio, R., Tafsili, M.A.B., dan Slamet. (2018). Treatment of Batik Industry Waste with a Combination of Electrocoagulation and Photocatalysis. *International Journal of Technology*. 9(5): 936-943.

[2] Birgani, P. M., Ranjbar, N., Abdullah, R. C., Wong, K. T., Lee, G., Ibrahim, S., Park, C., Yoon, Y., & Jang, M. (2016). An Efficient and Economical Treatment for Batik Textile Wastewater Containing High Levels of Silicate and Organic Pollutants Using a Sequential Process of Acidification, Magnesium Oxide, and Palm Shell-Based Activated Carbon Application. *Journal of Environmental Management*. 184: 229–239. https://doi.org/10.1016/j.jenvman.2016.09.066

[3] Sutisna, S., Wibowo, E., Rokhmat, M., Rahman, D. Y., Murniati, R., Khairurrijal, K., & Abdullah, M. (2017). Batik Wastewater Treatment Using TiO_2 Nanoparticles Coated on the Surface of Plastic Sheet. *Procedia Engineering*. 170: 78–83. https://doi.org/10.1016/j.proeng.2017.03.015

[4] Budiyanto, S., Purnaweni, H., & Sunoko, H. R. (2018). Environmental analysis of the impacts of batik waste water polution on the quality of dug well water in the batik industrial center of Jenggot Pekalongan City. In *E3S Web of Conferences* (Vol. 31, p. 09008). EDP Sciences.

[5] Azha, S. F. & Ismail S. (2021). Feasible and Economical Treatment of Real Hand-Drawn Batik/Textile Effluent Using Zwitterionic Adsorbent Coating: Removal Performance and Industrial Application Approach. *Journal of Water Process Engineering*. 41 (102093). https://doi.org/10.1016/j.jwpe.2021.102093

[6] Mukimin A., Vistanty H., Zen N., Purwanto, A., & Wicaksono K.A. (2018). Performance of Bioequalizationelectrocatalytic Integrated Method for Pollutants Removal of Hand-Drawn Batik Wastewater. *Journal of Water Process Engineering*. 21: 77-83. https://doi.org/10.1016/j.jwpe.2017.12.004

[7] Dwisandi, R. F., Mutiara, F., Nurfauziah, E., & Meylani, V. (2021). Review effectiveness of indigenous local microorganisms in degrading hexavalent chromium (Cr (VI)) in Batik liquid waste. *Biological Environment and Pollution*, *1*(1), 19-29.

[8] Daud, N. M., Abdullah, S. R. S., Hasan, H. A., & Dhokhikah, Y. (2022). Integrated physical-biological treatment system for batik industry wastewater: A review on process selection. *Science of The Total Environment*, *819*, 152931.

[9] Febriasari, A., Huriya, Ananto, A. H., Suhartini, M., & Kartohardjono, S. (2021). Polysulfone–polyvinyl pyrrolidone blend polymer composite membranes for

batik industrial wastewater treatment. *Membranes*, *11*(1), 66.

[10] Kuvarega, A. T., & Mamba, B. B. (2016). Photocatalytic Membranes for Efficient Water Treatment. *Semiconductor Photocatalysis - Materials, Mechanisms and Applications*. InTech. https://doi.org/10.5772/62584

[11] Notodarmodjo, S., Gustiani, S., Radiman, C., & Syafila, M. (2016). Pengaruh Fouling pada Permukaan Membran Serat Nano Selulosa Bakterial Dengan Fotokatalis Ag dan TiO_2. *Arena Tekstil,* 31(1), 35–42. https://doi.org/10.31266/at.v31i1.1445

[12] Alyarnezhad, S., Marino, T., Parsa, J. B., Galiano, F., Ursino, C., Garcìa, H., Puche, M., & Figoli, A. (2020). Polyvinylidene Fluoride-Graphene Oxide Membranes for Dye Removal Under Visible Light Irradiation. *Polymers*, 12(7), 1–19. https://doi.org/10.3390/polym12071509

[13] Kusworo, T. D., Dalanta, F., Aryanti, N., & Othman N. H. (2021). Intensifying Separation and Antifouling Performance of PSf Membrane Incorporated by GO and ZnO Nanoparticles for Petroleum Refinery Wastewater Treatment. *Journal of Process Engineering.* 41 (102030).

[14] Feng, H., Xu, H., Feng, H., Gao, Y., & Jin, X. (2019). The Sol-Gel Synthesis and Photocatalytic Activity of Gd-SiO_2-TiO_2 Photocatalyst. *Chemical Physics Letters*. 733: 136676.

[15] Kusworo, T. D., Aryanti, N., Qudratun, & Utomo, D. P. (2018). Oilfield produced water treatment to clean water using integrated activated carbon-bentonite adsorbent and double stages membrane process. *Chemical Engineering Journal*, *347*, 462–471. https://doi.org/10.1016/j.cej.2018.04.136

[16] Estikarini, H. D., Hadiwidodo, M., & Luvita, V. (2016). Penurunan Kadar COD dan TSS pada Limbah Tekstil dengan Metode Ozonasi*. Jurnal Teknik Lingkungan*, Vol 5, No. 1.

[17] El-Zahhar, A. A., Idris, A. M., Fawy, K. F., & Arshad, M. (2021). SEM, SEM-EDX, μ-ATR-FTIR and XRD for urban street dust characterisation. *International journal of environmental analytical chemistry*, *101*(7), 988-1006.

[18] Humairo, F. Y. (2015). Preparasi dan Karakterisasi Membran Serat Berongga PVDF/PEG400-TiO_2 untuk Pemisahan Limbah Sintetik Air-Minyak. *Doctoral Dissertation*. Institut Teknologi Sepuluh Nopember.

[19] Sanjaya, H. (2017). Degradasi Methylene Blue Menggunakan Katalis Zno-Peg Dengan Metode Fotosonolisis. *Eksakta: Berkala Ilmiah Bidang MIPA* (E-ISSN: 2549-7464). 18(02): 21-29.

[20] Cheng, S., Zhao, S., Xing, B., Liu, Y., Zhang, C., & Xia, H. (2022). Preparation of magnetic adsorbent-photocatalyst composites for dye removal by synergistic effect of adsorption and photocatalysis. *Journal of Cleaner Production*, *348*, 131301.

[21] Kusworo, T.D., Andri C. K., Nita A., Tonni A. K., Febio D., Nur H. A. (2023). Photocatalytic polysulfone membrane incorporated by ZnO-MnO2@SiO2 composite under UV light irradiation for the reliable treatment of natural rubber-laden wastewater. *Chemical Engineering Journal.* 451: 1. https://doi.org/10.1016/j.cej.2022.138593

[22] Xu, Z., Wu, T., Shi, J., Teng, K., Wang, W., Ma, M., Li, J., Qian, X., Li, C., & Fan, J. (2016). Photocatalytic antifouling PVDF ultrafiltration membranes based on synergy of graphene oxide and TiO_2 for water treatment. *Journal of Membrane Science*. 520: 281–293. https://doi.org/10.1016/j.memsci.2016.07.060

[23] Pophali, G. R., Hedau, S., Gedam, N., Rao, N. N., & Nandy, T. (2011). Treatment of refractory organics from membrane rejects using ozonation. *Journal of Hazardous Materials,* 189(1–2), 273–277. https://doi.org/10.1016/j.jhazmat.2011.02.030

[24] Yuan, Y and Lee, T. R. (2013). Contact Angle and Wetting Properties, Surface Science Techniques. *Springer,* 3–34.

[25] Psaltou, S., & Zouboulis, A. (2020). Catalytic ozonation and membrane contactors—a review concerning fouling occurrence and pollutant removal. *Water (Switzerland),* 12(11), 1–34. https://doi.org/10.3390/w12112964

[26] Dewanti, B. S. D., Prastiwi, T. F., & Sutan Haji, A. T. (2019). Pengolahan Limbah Cair Batik Menggunakan Kombinasi Metode Netralisasi Dan Elektrokoagulasi. Jurnal Rekayasa Dan Manajemen Agroindustri, 7(3), 358. https://doi.org/10.24843/jrma.2019.v07.i03.p03

[27] Andrunik, M., Tomasz Bajda. (2019). Modification of Bentonite with Cationic and Nonionic Surfactants: Structural and Textural Features. Materials, 12 (22): 3772. https://doi.org/10.3390/ma12223772

[28] Chen, N., Chen, S., Yin, H., Zhu, B., Liu, M., Yang, Y., ... & Wei, G. (2023). Durable underwater super-oleophobic/super-hydrophilic conductive polymer membrane for oil-water separation. *Water Research*, *243*, 120333.

[29] Yang, F., Huang, J., Deng, L., Zhang, Y., Dang, G., & Shao, L. (2022). Hydrophilic modification of poly (aryl sulfone) membrane materials toward highly-efficient environmental remediation. *Frontiers of Chemical Science and Engineering*, 1-20.

[30] Sutrisna, P. D., Kurnia, K. A., Siagian, U. W., Ismadji, S., & Wenten, I. G. (2022). Membrane fouling and fouling mitigation in oil–water separation: A review. *Journal of Environmental Chemical Engineering*, *10*(3), 107532.

[31] Lee, Y., Kim, T., Kim, B., Choi, S., & Kim, K. (2023). Synthesis of TiO2/MoSx/Ag nanocomposites via photodeposition for enhanced photocatalysis and membrane fouling mitigation. *Journal of Environmental Chemical Engineering*, *11*(2), 109266.

[32] Baig, N., Salhi, B., Sajid, M., & Aljundi, I. H. (2022). Recent progress in microfiltration/ultrafiltration membranes for separation of oil and water emulsions. *The Chemical Record*, *22*(7), e202100320.